Rare regions of the susceptible-infected-susceptible model on Barabási-Albert networks

Géza Ódor

Research Centre for Natural Sciences, Hungarian Academy of Sciences, MTA TTK MFA, P.O. Box 49, H-1525 Budapest, Hungary

(Received 28 January 2013; revised manuscript received 5 April 2013; published 29 April 2013)

I extend a previous work to susceptible-infected-susceptible (SIS) models on weighted Barabási-Albert scale-free networks. Numerical evidence is provided that phases with slow, power-law dynamics emerge as the consequence of quenched disorder and tree topologies studied previously with the contact process. I compare simulation results with spectral analysis of the networks and show that the quenched mean-field (QMF) approximation provides a reliable, relatively fast method to explore activity clustering. This suggests that QMF can be used for describing rare-region effects due to network inhomogeneities. Finite-size study of the QMF shows the expected disappearance of the epidemic threshold λ_c in the thermodynamic limit and an inverse participation ratio ∼0.25, meaning localization in case of disassortative weight scheme. Contrarily, for the multiplicative weights and the unweighted trees, this value vanishes in the thermodynamic limit, suggesting only weak rare-region effects in agreement with the dynamical simulations. Strong corrections to the mean-field behavior in case of disassortative weights explains the concave shape of the order parameter $\rho(\lambda)$ at the transition point. Application of this method to other models may reveal interesting rare-region effects, Griffiths phases as the consequence of quenched topological heterogeneities.

DOI: 10.1103/PhysRevE.87.042132 PACS number(s): 05.70.Ln, 89.75.Hc, 89.75.Fb

I. INTRODUCTION

The research of nonequilibrium models has been a central topic of statistical mechanics [1–3]. A fundamental dynamical model to understand them is the contact process (CP) [4,5], in which sites can be either active (infected) or inactive (susceptible). By decreasing the infection rate of the neighbors λ/k, where k is the degree of the vertex, a continuous phase transition occurs at some λ_c critical point from the active to the inactive steady state. The latter is also called absorbing, because no spontaneous activation of sites is allowed and the density of infection (ρ) is zero.

Recently the interest has been shifted from models, defined on Euclidean, regular lattices to processes living on general networks [6,7]. The effects of the heterogeneous topological structures [8,9] is not yet fully understood. In particular, in the case of ubiquitous scale-free (SF) networks [10], exhibiting $P(k) \sim k^{-\gamma}$ degree distribution of the nodes [6,7] the location of the phase transition and the singular behavior is still a debated issue. Numerical simulations [11–14] and theoretical approaches based on the heterogeneous mean-field (HMF) theory [11,12,15] show strong effects of the network heterogeneity on the behavior of the CP defined on complex networks.

Although SF-s exhibit infinite topological dimension (d), defined by $N \propto r^d$, where N is the number of nodes within the (chemical) distance r, simple mean-field approximations cannot capture several important features. Studies of the CP, as well as other processes [8,9], have shown that quenched disorder in networks is relevant in the dynamical systems defined on top of them. Very recently it has been shown [16–18] that generic slow (power-law or logarithmic) dynamics is observable by simulating CP on networks with finite d. This observation is relevant for recent developments in dynamical processes on complex networks such as the simple model of "working memory" [19], brain dynamics [20], social networks with heterogeneous communities [21], or slow relaxation in glassy systems [22].

Slow dynamics can be the consequence of bursty behavior of agents connected by small world networks resulting in memory effects [23]. An independent cause is related to arbitrarily large ($l < N$), active rare-regions (RR) with long lifetimes: $\tau \propto \exp(l)$ in the inactive phase ($\lambda \leqslant \lambda_c$). In the region $\lambda_c^0 < \lambda < \lambda_c$, where λ_c^0 is the critical point of the impure system, a so-called Griffiths phase (GP) [24,25] develops, with algebraic density decay $\rho \propto t^{-\alpha}$, α being a nonuniversal exponent. At and below the λ_c^0 rare clusters may still form, with an over-average mean degree, which are locally supercritical at a given λ and induce a slower-than-exponential but faster-than-power-law decay of the global density. In the case of these "weak rare-region effects," numerical simulations [18] showed stretched-exponential decay, $\rho(t) \sim e^{-\text{const}\times t^y}$ with exponents y varying from values close to 1, for small λ, to very small values (converging to 0) for λ approaching the GP. The rare-region induced dynamical behavior can be described by nonperturbative methods [26–29].

More recently, the possibility of slow dynamics has been investigated on Barabási-Albert (BA) networks with $\gamma = 3$, possessing infinite d [30]. Very extensive simulations showed linear leading order density decay and $\rho(\lambda, t \to \infty) \propto |\lambda - \lambda_c|$ behavior with logarithmic corrections, in agreement with the HMF approximations. It was also pointed out that in the case of BA networks with one link per incoming node the epidemic propagation slows down, and nontrivial critical density decay emerges with $\rho(t, \lambda_c) \propto t^{-\alpha}$, $\alpha \simeq 0.5$. Furthermore, when k-dependent weighting was also applied, suppressing hubs or making the network disassortative, GP-like regions could be observed in the simulations. A systematic finite scaling study revealed that these power-laws saturate in the $N \to \infty$ thermodynamic limit, suggesting smeared phase transitions [25]. This can be understood via the possibility of embedding even infinite dimensional, active RR-s in networks with $d = \infty$, leading to finite steady-state density: $\rho(t \to \infty, N \to \infty)$. A numerical percolation analysis [30] has strengthened this view indeed.

I continue the work [30] to explore whether quenched mean-field (QMF) theory [31] with spectral decomposition (SD) can help understanding rare-region effects in complex networks. The QMF differs from HMF by taking into account variations of the quenched network topology. I study the susceptible-infected-susceptible (SIS) model [32] instead of the CP, because the infection rate is independent of k; thus, the rate equation involves symmetric matrices and a spectral analysis can be done on an orthonormal basis with real, nonnegative eigenvalues. The SIS model is a two-state system in which infected sites propagate the epidemic (venerate all neighbors) with rate λ or recover with rate 1.

This extension is far from trivial because the epidemic transmitting capability of the infected nodes is higher than in CP; i.e., it is not normalized by the number of outgoing edges. Therefore, the emergence of localized rare regions (RR) is more difficult. I provide extensive simulation results, showing numerical evidence for GP-like regions with generic slow dynamics, similarly as in case of the CP. The QMF and SD analysis set up for these cases is in good agreement with the dynamical simulations.

II. NETWORK MODELS

I consider here SIS on BA networks, in particular for loop-less and weighted cases as described in Ref. [30]. This permits very simple and fast construction, in contrast with other standard network generation models; e.g., see Ref [33]. The BA growth starts with a fully connected graph of size $N_0 = 10$ nodes, but comparisons with $N_0 = 5$ and 20 have also been done to test any dependence. For BA at each time step s, a new vertex (labeled by s) with m edges is added to the network and connected to an existing vertex s' of degree $k_{s'}$ with probability $\Pi_{s\to s'} = k_{s'}/\sum_{s''=1}^{s''<s} k_{s''}$. This process is iterated until reaching the desired network size N. The resulting network has a SF degree distribution $P(k) \simeq k^{-3}$. For $m = 1$ we obtain a BA tree (BAT) topology, while for the looped case, $m = 3$ was applied.

Binary (nonweighted) BA networks have been transformed to weighted ones by assigning to every edge connecting vertexes i and j a symmetric weight ω_{ij}. In Ref. [30], two different network topology-dependent quenched weight assignment strategies were introduced in order to slow down and localize epidemics.

(i) *Weighted BA tree I (WBAT-I).* Multiplicative weights, suppressing the infection capability of highly connected nodes

$$\omega_{ij} = \omega_0 (k_i k_j)^{-\nu}, \tag{1}$$

where ω_0 is an arbitrary scale and ν is a characteristic exponent with $\nu \geqslant 0$. This can model internal limitations of hubs, like the sublinear Heap's law [34]. In this paper, I study the case with $\nu = 1.5$ exponent.

(ii) *Weighted BA tree II (WBAT-II).* Disassortative weighting scheme according to the age of nodes in the network construction

$$\omega_{ij} = \frac{|i-j|^x}{N}, \tag{2}$$

where the node numbers i and j correspond to the time step when they were connected the network. Since the degree of nodes decreases as $k_i \propto (N/i)^{1/2}$ during this process, this selection with $x > 0$ favors connection between unlike nodes and suppresses interactions between similar ones. In Ref. [30], simulations showed evidence for a phase with power-law dynamics of the CP for $x = 2,3$ with CP. This paper is concerned about $x = 2$ networks.

The presence of these weights affects the dynamics of the SIS. Thus, the rate at which a healthy vertex i becomes ill on contact with an infected (active) vertex j is proportional to $\lambda\omega_{ij}$; therefore, the epidemic can in principle become trapped in isolated connected subsets. These regions of size l are rare in general: $P(l) \propto \exp(-l)$ but can exhibit exponentially long lifetimes $\tau(l) \propto \exp(l)$. In the healthy (inactive) phase, they provide the leading order contribution to the density of infected sites

$$\rho(t) \sim \int l P(l) \exp(-t/\tau) dl, \tag{3}$$

which in the saddle point approximation results in $\rho(t) \sim t^{-\alpha}$ decay [16].

III. SPECTRAL ANALYSIS

In Ref. [30], the heterogeneous mean-field (HMF) analysis of CP was worked out for these network models. However, extensive simulations showed different dynamical behaviors, except from the looped BA CP model case. Since HMF can't take into account rare region effects, nor models on trees, that conclusion was not very surprising.

A mean-field theory, capable of describing the effects of quenched topologies of the network on which SIS is defined is expected to give better agreement with numerical simulations. The QMF approach is based on the rate equation for $\rho_i(t)$, the infection probability of node i at time t [31]:

$$\frac{d\rho_i(t)}{dt} = -\rho_i(t) + [1-\rho_i(t)] \sum_j A_{ij}\lambda\rho_j(t), \tag{4}$$

where A_{ij} is an element of the adjacency matrix assigned with 1, if there is an edge between nodes i and j or 0 otherwise. This equation can be generalized by replacing the adjacency matrix with the weighted adjacency matrix $B_{ij} = A_{ij}\omega_{ij}$, having weighted elements: $B_{ij} \in [0,1]$.

For $t \to \infty$, the system evolves into a steady state, with the probabilities expressed as

$$\rho_i = \frac{\lambda \sum_j B_{ij}\rho_j}{1 + \lambda \sum_j B_{ij}\rho_j}. \tag{5}$$

Stability analysis shows that $\rho_i > 0$ above a λ_c epidemic threshold, with finite-order parameter (prevalence) $\rho \equiv \langle \rho_i \rangle$.

In the SD approach one expands ρ_i in the space of eigenvectors of the adjacency matrix A_{ij} (or B_{ij} for weighted case) as

$$\rho_i = \sum_\Lambda c(\Lambda) f_i(\Lambda). \tag{6}$$

This extension can be done for real and symmetric weights, when the eigenvectors $\boldsymbol{f}(\Lambda)$ span a complete orthonormal basis. For nonnegative, symmetric matrices extension of the Perron-Frobenius theorem asserts that it exhibits real eigenvalues, furthermore the largest one $\Lambda_{\max} \equiv \Lambda_1 \geqslant \Lambda_2 \geqslant \ldots \Lambda_N$

is unique and that the corresponding eigenvector $\boldsymbol{f}(\Lambda_1)$ has nonnegative components. In this basis, Eq. (5) can be expressed by the coefficients $c(\Lambda)$ as

$$c(\Lambda) = \lambda \sum_{\Lambda'} \Lambda' c(\Lambda') \sum_{i=1}^{N} \frac{f_i(\Lambda) f_i(\Lambda')}{1 + \lambda \sum_{\widetilde{\Lambda}} \widetilde{\Lambda} c(\widetilde{\Lambda}) f_i(\widetilde{\Lambda})}. \quad (7)$$

This gives $\lambda_c = 1/\Lambda_1$ for the epidemic threshold and in its neighborhood the order parameter can be approximated by the eigenvectors of the largest eigenvalues,

$$\rho(\lambda) \approx a_1 \Delta + a_2 \Delta^2 + ..., \quad (8)$$

where $\Delta = \lambda\Lambda_1 - 1 \ll 1$, with the coefficients [35]

$$a_j = \sum_{i=1}^{N} f_i(\Lambda_j) / \left[N \sum_{i=1}^{N} f_i^3(\Lambda_j) \right]. \quad (9)$$

A homogeneous solution implies that a finite fraction of vertexes are infected right above λ_c and a_1 is the order of $O(1)$. That would mean that the components of $\boldsymbol{f}(\Lambda_1)$ are localized. On the other hand, quenched inhomogeneous topologies can also imply inhomogeneous ρ_i distributions and one can assume that they result in rare region effects, as in Refs. [16–18,30].

To describe localization in the components of $\boldsymbol{f}(\Lambda_1)$, Ref. [31] suggested to use the inverse participation ratio

$$\mathrm{IPR}(\Lambda) \equiv \sum_{i=1}^{N} f_i^4(\Lambda), \quad (10)$$

which in the limit $N \to \infty$ is of the order of $O(1)$ when the eigenvector is localized. Contrary, when $\mathrm{IPR}(\Lambda) \to 0$, this state is delocalized. Equation (9) implies that for localized principal eigenvector $a_1 \sim O(1/N)$, thus $\rho \approx a_1 \Delta \sim O(1/N)$, the disease is localized on a finite number $N\rho$ of vertexes. On the other hand, when $\boldsymbol{f}(\Lambda_1)$ is delocalized, the disease infects a finite fraction of vertexes for $\lambda > \lambda_c$.

Goltsev *et al.* [31] analyzed artificial and real SF networks and found that in the case of localized cases, the epidemic threshold was actually absent and a real epidemic affecting a finite fraction of vertexes occurred after a smooth crossover at higher values of λ. This is in agreement with the smeared phase transition scenario proposed to explain the numerical results for CP on weighed BA trees in Ref. [30]. In those systems, rare-regions effects seemed to arise, causing power-law density decays, which ultimately crossed over to saturation to finite ρ-s in the $N \to \infty$ limit. Right above λ_c similar concave shaped $\rho(\lambda)$ was obtained as in the localized cases of Ref. [31]. Here I investigate the situation for SIS instead of CP models, to see if this relation holds on. This has been done using finite-size scaling analysis of the quantities: $\lambda = 1/\Lambda_1$, IPR and a_i for $i = 1,2,3$.

It has been proven [36] that for random, unweighted SF networks, with power-law degree distribution $P(k) \propto k^{-\gamma}$ the maximal eigenvalue scales as $\Lambda_1 \propto \sqrt{k_{\max}}$ for $\gamma > 2.5$. Furthermore, the maximal degree of the network satisfies $k_{\max} = \min[N^{1/2}, N^{1/(\gamma-1)}]$, due to the structural cutoff of a finite network with $\gamma \leqslant 3$. Therefore, Λ_1 should scale with the network size as

$$\Lambda_1(N) \propto N^{1/4} \quad (11)$$

for $\gamma = 3$ considered here.

TABLE I. Spectral QMF analysis results for SIS in different networks

Network	λ	c	IPR	a_1	a_2	a_3
BA	0.02(3)	0.32(4)	0.015(3)	4×10^{-4}	10^{-7}	10^{-8}
BAT	$-0.001(2)$	0.24(1)	0.06(1)	10^{-4}	10^{-7}	10^{-9}
WBAT-I	0.0001(3)	0.9(1)	0.001(2)	0.35(1)	5×10^{-8}	10^{-6}
WBAT-II	0.001(1)	0.23(2)	0.23(2)	4×10^{-3}	3×10^{-5}	10^{-3}

Using the software package OCTAVE I [37] generated the B_{ij} matrices of BA, BAT, WBAT-I, and WBAT-II networks for several sizes up to $N = 200.000$ and calculated the three largest eigenvalues and the corresponding eigenvectors. From these I deduced $1/\Lambda_1$, IPR, and a_i. The whole SD analysis was done using the sparse matrix functions of OCTAVE to handle B_{ij}-s of the networks within reasonable computing times. For the largest sizes, 1–2 weeks of a CPU time was needed. Least-squares fitting with the form

$$1/\Lambda_1 = \lambda_c + X(1/N)^c \quad (12)$$

has been applied for the largest eigenvalues. As Table I shows, a good agreement was obtained with the finite size scaling expectation $\lim_{N\to\infty} 1/\Lambda_1 = \lambda_c = 0$ of the QMF method. The $N \to \infty$ extrapolated critical threshold values converge to zero using the three parameter fitting form Eq. (12). The fitted power c agrees with an exponent of Eq. (11) reasonably well, except from the WBAT-I case, where QMF results for only $N \leqslant 6000$ could be achieved.

The IPR values decrease with $1/N$ and remain very small for the unweighted BA (IPR < 0.02) and BAT (IPR < 0.07) networks, albeit in the latter case the tendency seems to change for $N \geqslant 32\,000$ as shown on Fig. 1. This suggests an agreement with the anomalous scaling behavior of CP on the BA tree reported in Ref. [30]. Here, some clustering may be expected,

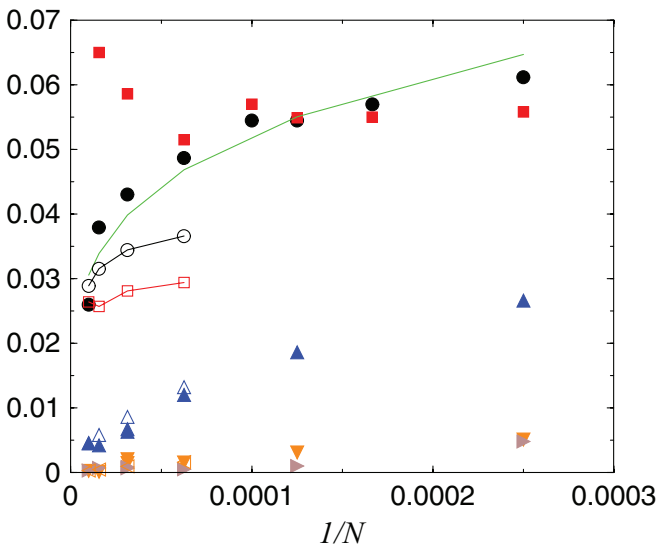

FIG. 1. (Color online) Finite-size scaling of QMF SD results for BAT model for $N = 4000$, 8000, 16 000, 32 000, 64 000, 100 000. Bullets, λ_c; boxes, IPR; up-triangles, a_1; down-triangles, a_2; right-triangles, a_3. Lines: least-squares fitting for with the form Eq. (12). Closed symbols correspond to $N_0 = 10$; open ones to $N_0 = 20$.

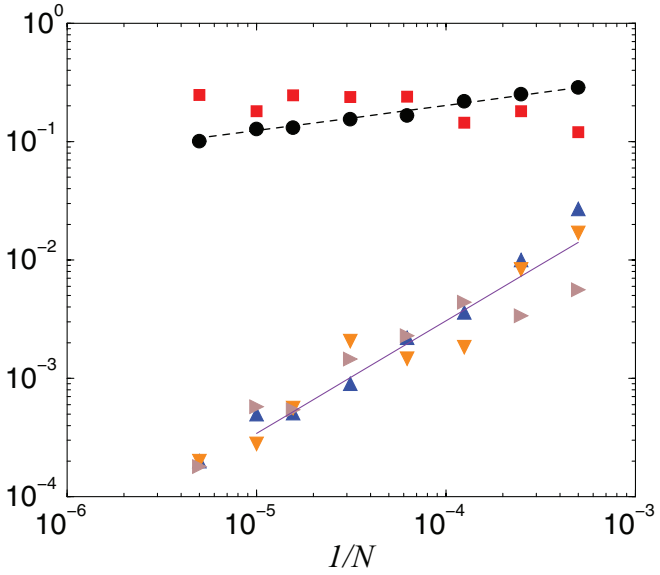

FIG. 2. (Color online) Finite-size scaling of QMF SD results for WBAT-II model for $N = 2\,000, 4\,000, \ldots 200\,000$. Bullets, λ_c; boxes, IPR; up-triangles, a_1; down-triangles, a_2; right-triangles, a_3. Lines: least-squares fitting for with the form Eq. (12).

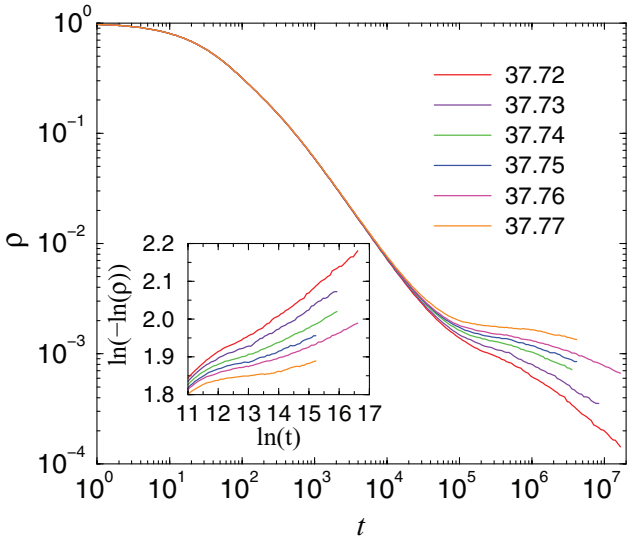

FIG. 3. (Color online) Density decay as a function of time for the SIS model on weighted BA trees generated with the WBAT-I scheme with exponent $\nu = 1.5$. Network size $N = 2 \times 10^6$. Different curves correspond to $\lambda = 37.72, 37.73, 37.74, 37.75, 37.76, 37.77$ (from bottom to top). Inset: The same data plotted on the $\ln\{-\ln[\rho(t)]\}$ vs. $\ln(t)$ scale (with parameters from top to bottom order).

which should be checked further by studying networks with $N \gg 10^5$ nodes. Unfortunately, this is out of the scope of the present study using OCTAVE but is in preparation using high performance graphics cards. For the WBAT-II case, IPR stabilizes to $\simeq 0.23(2)$ (see Fig. 2), advocating strong epidemic localization.

One can speculate that the initial compact seeds, from which the BA graphs originate, can influence the clustering behavior of the epidemic in the steady state. By varying the seed size, $N_0 = 5, 10, 20$, no measurable effects were found on the WBAT results. For the unweighted BA and BAT networks one can see differences between the finite-size results of the $N_0 = 20$ and $N_0 = 10$ cases (see Fig. 1), but the $N \to \infty$ asymptotic behavior appears to be the same.

For the unweighted BA and BAT networks, the eigenvalue analysis provides $a_1 \gg a_2 \gg a_3$ for all sizes in agreement with the $\beta = 1$ HMF results for ρ slightly above the critical threshold. In the $N \to \infty$ limit, $a_1(N) \sim (1/N)^{0.5}$ and $a_2 \simeq a_3 \simeq 0$ already for small sizes. For the weighted WBAT-I case, a_1 remains constant $\sim 0.35(1)$ while $a_2 \sim a_3 \sim (1/N)$. In the case of the WBAT-II tree, a_i are of the same order of magnitude and vanish linearly with $1/N$ (see Fig. 2), meaning a strong corrections to the leading-order linear scaling. When one plots $\rho(\lambda)$ with these values, one gets a concave curve from above and a tangential approach to λ_c. Such steady-state behavior has already been seen by simulations of CP on weighted BA networks [38]. In the next section, I compare these QMF results with simulations of SIS on WBAT-I and WBAT-II networks.

IV. SIS MODEL SIMULATIONS ON WEIGHTED TREES

In simulations, I considered the SIS model in continuous time as in Ref. [39], to be in accordance with the rate equations. At each time step, a randomly chosen infected node recovers with probability $n_i/(n_i + \lambda n_n)$, where n_i is the the number of infected nodes and n_n is the total number of links emanating from them. Complementary, one of the links is selected and the infection is transmitted, with probability $\lambda n_i/(n_i + \lambda n_n)$. Following the reaction, N_i and N_n are updated and the time is incremented by $\Delta t = 1/(n_i + \lambda n_n)$. The time is measured by these Monte Carlo steps (MCs) and shown to be dimensionless on the figures. These processes are iterated until $t < t_{\max}$ or until the epidemic stops ($N_i = 0$).

The networks were generated via the BA linear preferential attachment rule [10], following an initial fully connected seed of $N_0 = 20$. Neighbor indices of sites are stored in a dense matrix to save memory; thus, up to $N = 6 \times 10^6$-sized networks could be studied. The initial state was fully active and the concentration of infected sites was followed up to $t_{\max} = 4 \times 10^6$ MCs. Density decay runs were repeated and averaged over $\sim 10^4$ and up to 10^5 independent network realizations for WBAT-I and WBAT-II, respectively. I have also calculated the effective decay exponents, defined as the local slopes of $\rho(t)$ as given by

$$\alpha_{\text{eff}}(t) = -\frac{\ln[\rho(t)/\rho(t')]}{\ln(t/t')}, \tag{13}$$

where t and t' have been chosen in such a way that the discrete approximate of the derivative is sufficiently smooth. The static scaling behavior in the active steady state has also been investigated by measuring $\rho(\lambda, t \to \infty)$ deep in the saturation region.

Figure 3 suggests that $\rho(t)$ of the WBAT-I model exhibits λ-dependent power-laws for $t > 3 \times 10^5$ MCs. This can be observed in networks with $N = 2 \times 10^6$ nodes in the region $37.72 \leqslant \lambda \leqslant 37.77$. The final slope at the lowest $\lambda = 37.72$ power-law curve is $\alpha \simeq 0.343(4)$. By increasing the system size, these curves become ultimately constant, as in the case of the CP [30], meaning that the transition smears in the

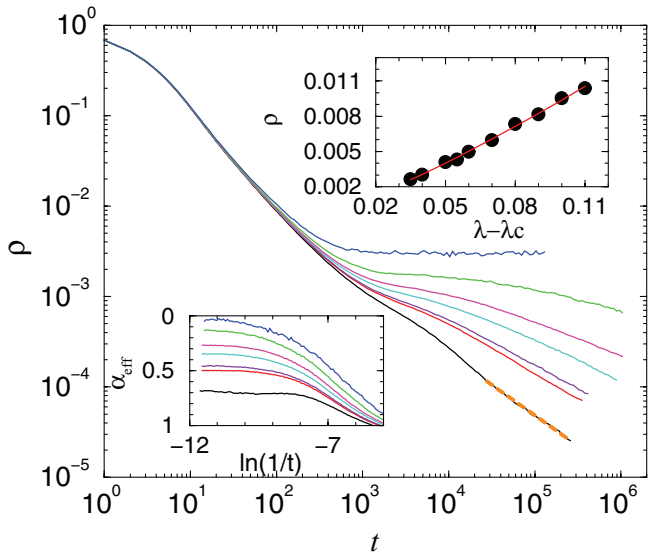

FIG. 4. (Color online) Density decay as a function of time for the SIS on weighted BA trees generated with the age-dependent (disassortative) WBAT-II scheme with exponent $x = 2$. Network size $N = 10^6$. Different curves correspond to $\lambda = 1.657$, 1.66, 1.661, 1.663, 1.67, 1.68, 1.69 (from bottom to top). Dashed line: power-law fit. Left inset: Local slopes of the same curves showing level-off for large times. Right inset: Steady-state density (bullets) above the epidemic threshold. The line shows power-law fitting with the form Eq. (14).

thermodynamic limit. However, the above range is narrow both in λ and the effective exponent α. Furthermore, some down curvature can also be seen on the log-log plots in this region, which makes the power-law dynamics assumption questionable. Since the QMF SD analysis suggests only weak rare-region effects, I plotted the same data on the $\ln\{-\ln[\rho(t)]\}$ versus $\ln(t)$ scale. As the inset of Fig. 3 shows, straight lines appear asymptotically, corresponding to stretched exponential decay behavior. In comparison, CP power laws with $0.3 \leqslant \alpha \leqslant 1$ could be seen clearly in the region $140 \leqslant \lambda \leqslant 145$ [30].

In the case of WBAT-II network, power-laws decays of $\rho(t,\lambda)$ appear already for $t > 50.000$ MCs as shown in Fig. 4. To see corrections to scaling, I have plotted the effective decay exponents Eq. (13) in the left inset of Fig. 4. The final slope of the lowest $\lambda = 1.657$ curve tends to $\alpha \simeq 0.70(2)$, which is far away from the HMF critical exponent value: $\alpha = 1$. The dynamical scaling behavior appears in the $1.657 \leqslant \lambda < 1.68$ region, at much lower infection rates than in the case of the CP [30]. However, a smeared transition is expected again, since the densities in the steady state $\rho(t \to \infty)$ increase with N. As the inset of Fig. 4 shows, $\rho(\lambda, t \to \infty)$ can be fitted using

$$\rho(\lambda, t \to \infty) = C(\lambda - \lambda_c)^{\beta}, \tag{14}$$

with an order parameter exponent $\beta = 1.22(1)$ near $\lambda_c = 1.64(1)$ for networks with size $N = 4 \times 10^6$.

V. DISCUSSION AND CONCLUSIONS

Understanding effects of heterogeneities in nonequilibrium, dynamical systems is a challenging open field. References [16,18] concluded that finite topological dimension is a necessary condition for observing Griffiths phases and activated scaling in the case of the basic model of nonequilibrium system, the contact process. In the case of CP on certain weighed networks, numerical evidence was shown for generic power laws, but in the thermodynamic limit this phase seems to disappear and a smeared phase transition exists, due to the infinite-dimensional correlated rare regions [30]. In contrast with these, strong disorder renormalization studies of the random transverse-field Ising model found Griffiths singularities [40] even in the infinite-dimensional Erdős-Rényi random graphs [41].

Very recently, Griffiths phases have been reported in a study of the random transverse Ising model on complex networks with a scale-free degree distribution regularized by and exponential cutoff $p(k) \propto k^{-\gamma} \exp[-k/\xi]$ [42]. This model was devised to understand the relation between the onset of the superconducting state with the particular optimum heterogeneity in granular superconductors. On quenched networks, a phase transition at zero temperature and a Griffith phase with decreasing size as the function of the cutoff ξ was found. The scenario is similar to our case, because increasing the value of the cutoff is like going to the thermodynamic limit of the SF network. Another fresh model study [43] argues again for the existence of GP in the SIS model defined on unclustered, deterministic SF networks, with $\gamma > 3$, below the percolation threshold of the network.

In this work, I provided spectral decomposition and QMF approximation to SIS models on different scale-free networks. This analysis has been supplemented with extensive numerical simulations showing dynamical effects of the topological disorder. Activity localization of the eigenvectors characterized by the IPR number predicts strong rare-region effects in the case of weighted WBAT-II trees. Numerical simulations exhibit a λ parameter region, with continuously changing power-laws decays. Still, in the $N \to \infty$ limit the $\rho(t)$ curves saturate, as for smeared phase transitions, discussed in Ref. [30]. For the WBAT-I tree, the picture is less clear. There is a narrow GP-like region at very late times ($t > 3 \times 10^5$ MCs), but the $\ln\{\rho[\ln(t)]\}$ curves exhibit downward curvature and stretched exponential dynamics looks more reasonable. This scenario is strengthened by the QMF SD analysis, which results in a vanishing IPR, suggesting only weak rare-region effects here. One can accept this because the neighbor infection in the SIS is more homogeneous than in the CP; thus, the disorder is weaker. This means that reducing the hub-hub weights is not enough in SIS to find strong rare region effects, but disassortativity can make the job.

This study goes one step further than Ref. [31] by analyzing spectral data of different graphs via finite size scaling. In particular, numerical evidence is shown for the disappearance of λ_c with the expected scaling law in the $N \to \infty$ limit. Fluctuations, omitted by the QMF approximation can be relevant, indeed simulations of SIS on finite graphs show $\lambda_c > 0$. However, finite-size study suggests $\lambda_c = 0$ in all cases, in accordance with smeared phase transition. Still the QMF SD analysis seems to be a relatively fast, promising way to explore topological rare-region effects, GPs in networks, especially with infinite topological dimension. Extension of this method for using more powerful numerical techniques is under way.

ACKNOWLEDGMENTS

I thank R. Pastor-Satorras, R. Juhász, and I. Kovács for useful discussions and acknowledge support from the Hungarian research fund OTKA (Grant No. T77629), HPC-EUROPA2 (Project No. 228398), and the European Social Fund through Project FuturICT.hu (Grant No. TAMOP-4.2.2.C-11/1/KONV-2012-0013).

[1] J. Marro and R. Dickman, *Nonequilibrium Phase Transitions in Lattice Models* (Cambridge University Press, Cambridge, 1999).
[2] G. Ódor, *Universality in Nonequilibrium Lattice Systems* (World Scientific, Singapore, 2008).
[3] M. Henkel, H. Hinrichsen, and S. Lübeck, *Non-equilibrium Phase Transition: Absorbing Phase Transitions* (Springer Verlag, Netherlands, 2008).
[4] T. E. Harris, Ann. Prob. **2**, 969 (1974).
[5] T. M. Liggett, *Interacting Particle Systems* (Springer-Verlag, New York, 1985).
[6] R. Albert and A.-L. Barabási, Rev. Mod. Phys. **74**, 47 (2002).
[7] S. N. Dorogovtsev and J. F. F. Mendes, *Evolution of Networks: From Biological Nets to the Internet and WWW* (Oxford University Press, Oxford, 2003).
[8] S. N. Dorogovtsev, A. V. Goltsev, and J. F. F. Mendes, Rev. Mod. Phys. **80**, 1275 (2008).
[9] A. Barrat, M. Barthélemy, and A. Vespignani, *Dynamical Processes on Complex Networks* (Cambridge University Press, Cambridge, 2008).
[10] A.-L. Barabási and R. Albert, Science **286**, 509 (1999).
[11] C. Castellano and R. Pastor-Satorras, Phys. Rev. Lett. **96**, 038701 (2006).
[12] C. Castellano and R. Pastor-Satorras, Phys. Rev. Lett. **100**, 148701 (2008).
[13] S. C. Ferreira, R. S. Ferreira, and R. Pastor-Satorras, Phys. Rev. E **83**, 066113 (2011).
[14] S. C. Ferreira, R. S. Ferreira, C. Castellano, and R. Pastor-Satorras, Phys. Rev. E **84**, 066102 (2011).
[15] M. Boguñá, C. Castellano, and R. Pastor-Satorras, Phys. Rev. E **79**, 036110 (2009).
[16] M. A. Muñoz, R. Juhász, C. Castellano, and G. Ódor, Phys. Rev. Lett. **105**, 128701 (2010).
[17] G. Ódor, R. Juhasz, C. Castellano, and M. A. Munoz, in *Nonequilibrium Statistical Physics Today*, Vol. 1332, edited by P. L. Garrido, J. Marro, and F. de los Santos (American Institute of Physics, College Park, MD, 2011), pp. 172–178.
[18] R. Juhász, G. Ódor, C. Castellano, and M. A. Muñoz, Phys. Rev. E **85**, 066125 (2012).
[19] S. Johnson, J. J. Torres, and J. Marro, PLoS ONE **8**, e50276 (2013).
[20] A. Haimovici, E. Tagliazucchi, P. Balenzuela, and D. R. Chialvo, Phys. Rev. Lett. **110**, 178101 (2013).
[21] X. Castelló, R. Toivonen, V. M. Eguíluz, J. Saramäki, K. Kaski, and M. San Miguel, Europhys. Lett. **79**, 66006 (2007).
[22] A. Amir, Y. Oreg, and Y. Imry, Phys. Rev. Lett. **105**, 070601 (2010).
[23] M. Karsai, M. Kivela, R. K. Pan, K. Kaski, J. Kertesz, A. L. Barabasi, and J. Saramaki, Phys. Rev. E **83**, 025102(R) (2011)
[24] R. B. Griffiths, Phys. Rev. Lett. **23**, 17 (1969).
[25] T. Vojta, J. Phys. A **39**, R143 (2006).
[26] A. J. Bray, Phys. Rev. Lett. **59**, 586 (1987).
[27] D. Dhar, M. Randeria, and J. P. Sethna, Europhys. Lett. **5**, 485 (1988).
[28] H. Rieger and A. P. Young, Phys. Rev. B **54**, 3328 (1996).
[29] D. S. Fisher, Phys. Rev. Lett. **69**, 534 (1992).
[30] G. Ódor and R. Pastor-Satorras, Phys. Rev. E **86**, 026117 (2012).
[31] A. V. Goltsev, S. N. Dorogovtsev, J. G. Oliveira, and J. F. F. Mendes, Phys. Rev. Lett. **109**, 128702 (2012).
[32] R. M. Anderson and R. M. May, *Infectious Diseases in Humans* (Oxford University Press, Oxford, 1992).
[33] M. Catanzaro, M. Boguñá, and R. Pastor-Satorras, Phys. Rev. E **71**, 027103 (2005).
[34] H. Heaps, *Information Retrieval: Computational and Theoretical Aspects* (Academic Press, Inc., Orlando, FL, 1978).
[35] P. Van Mieghem, Eur. Phys. Lett. **97**, 48004 (2012).
[36] F. Chung, L. Lu, and V. Vu, Proc. Natl. Acad. Sci. USA **100**, 6313 (2003).
[37] http://www.gnu.org/software/octave.
[38] M. Karsai, R. Juhász, and F. Iglói, Phys. Rev. E **73**, 036116 (2006).
[39] S. C. Ferreira, C. Castellano, and R. Pastor-Satorras, Phys. Rev. E **86**, 041125 (2012).
[40] I. A. Kovács and F. Iglói, J. Phys.: Condens. Matter **23**, 404204 (2011).
[41] P. Erdős and A. Rényi, Publicationes Mathematicae **6**, 290 (1959)
[42] G. Bianconi, J. Stat. Mech. (2012) P07021.
[43] H. K. Lee, P.-S. Shim, and J. D. Noh, arXiv:1211.2519.